npj | Quantum Materials

www.nature.com/npjquantmats

ARTICLE OPEN

Check for updates

Nanoscale studies of electric field effects on monolayer 1T′-WTe_2

Yulia Maximenko[1], Yueqing Chang[1], Guannan Chen[1], Mark R. Hirsbrunner[1], Waclaw Swiech[2], Taylor L. Hughes[1], Lucas K. Wagner[1] and Vidya Madhavan[1,2]✉

Monolayer 1 T′-WTe_2 is a quantum spin Hall insulator with a gapped 2D-bulk and gapless helical edge states persisting to temperatures ~100 K. Despite the far-ranging interest, the magnitude of the bulk gap, the effect of gating on the 2D-band structure, as well the role interactions are not established. In this work we use STM spectroscopy to measure the intrinsic bulk gap of monolayer 1 T′-WTe_2 and show that gate induced electric fields cause large changes of the gap magnitude. Our first-principles DFT-derived tight-binding model reveal that a combination of spatial localization of the conduction and valance bands and Rashba-like spin-orbit coupling leads to a gating induced spin-splitting of the 2D-bulk bands in the tens of meV, thereby reducing the band gap. Our work explains the large sensitivity of the band structure to electric fields and suggests a new avenue for realizing proximity induced non-trivial superconductivity in monolayer 1 T′-WTe_2.

npj Quantum Materials (2022)7:29 ; https://doi.org/10.1038/s41535-022-00433-x

INTRODUCTION

2D transition metal dichalcogenides present an exciting platform for realizing emergent phases having non-trivial topology and strong correlations, and are prime candidates for hosting topological edge states, topological superconductivity, and fractional excitations[1]. After more than a decade of intense search, monolayer WTe_2 (ML-WTe_2) (Fig. 1a–e) has recently emerged as a 2D time-reversal invariant topological insulator, i.e., a quantum spin Hall (QSH) insulator[2–5]. While bulk WTe_2 is a semimetal, band structure calculations of a monolayer indicate that it is a narrow-gap semiconductor exhibiting inverted bands that give rise to the QSH phase (Fig. 1f)[6,7]. Transport studies have confirmed quantized two-terminal edge conductance up to 100 K, and microwave impedance microscopy measurements have been used to observe edge states[8,9].

The simplest mechanism to tune the properties of 2D materials is by gating, i.e., the application of an electric field through a dielectric layer. Naively, gating may be expected to add or remove carriers from the film by shifting the bands with respect to the Fermi energy (rigid band shift) as is observed in graphene[10]. However, gating could have non-trivial effects on the band structure due to the presence of the out-of-plane electric field, or changes in effective screening. For example, out-of-plane electric fields break inversion symmetry and can lead to a spin splitting of the bands, like the Rashba effect. In WTe_2, electrostatic gating has been used to tune the circular photogalvanic effect[11] and induce an exotic superconducting phase[12,13]. Despite the far-ranging interest in this system and extensive transport studies, the exact gap size of ML-WTe_2, the dispersion of the edge states within the gap, as well as the effect of gating on the band structure have not yet been established. Indeed, the experimental literature reports a puzzlingly large variation in the observed gap sizes, which has yet to be explained[2,3,5,7,8,11–14]. Furthermore, recent studies have suggested that correlation effects may play a critical role in controlling band structure as well as gating dependent effects. Hence, comprehensive gating-dependent spectroscopic data is urgently needed to understand the key elements that control the low-energy physics of the system, and scanning tunneling microscopy (STM) and spectroscopy (STS) are ideal tools to probe gate-induced effects on the band structure and edge states.

In this work, we present a combined experimental-theoretical study on ML-WTe_2. High-quality monolayer WTe_2 films grown by molecular beam epitaxy (MBE) were studied by STM at 4 K. STM STS reveals clear bulk gaps with edge states that agree with density functional theory (DFT)—Heyd–Scuseria–Ernzerhof (HSE) calculations. We further find that the gap magnitude is highly tunable with gating. This gap tunability is quantitatively explained using a parameter-free first-principles DFT-derived tight-binding model. The calculations show that the conduction band states are predominantly located on the top and bottom layers with opposite spin-momentum locking, while the valence band states are localized to the interior tungsten layer. Application of an electric field changes the energy spacing between states in the three layers, resulting in a field-controllable spin-momentum selected gap.

RESULTS AND DISCUSSION

Film structure and topography

Monolayer WTe_2 has a distorted orthorhombic 1 T′ structure which preserves inversion symmetry (Fig. 1a). Figure 1b shows a large scale STM image of ML-WTe_2 grown on graphene on SiC. These films were transferred directly from the MBE to the STM using a vacuum suitcase (see Methods for details). Multiple monolayer islands of ~20–30 nm size, which correspond to the typical island size of MBE-grown WTe_2, can be seen in this field of view. Zooming into a representative island, we can resolve the characteristic stripes corresponding to protruding Te atoms of the top surface (for example, Fig. 1c, d). The observed lattice corresponds well to 1 T′-WTe_2. A representative bulk spectrum averaged over an area of 5 by 5 nm^2 on one island (Fig. 1e) exhibits a band gap of approximately 40 meV.

[1]Department of Physics, University of Illinois Urbana-Champaign, Urbana, IL 61801, USA. [2]Materials Research Laboratory, University of Illinois Urbana-Champaign, Urbana, IL 61801, USA. ✉email: vm1@illinois.edu

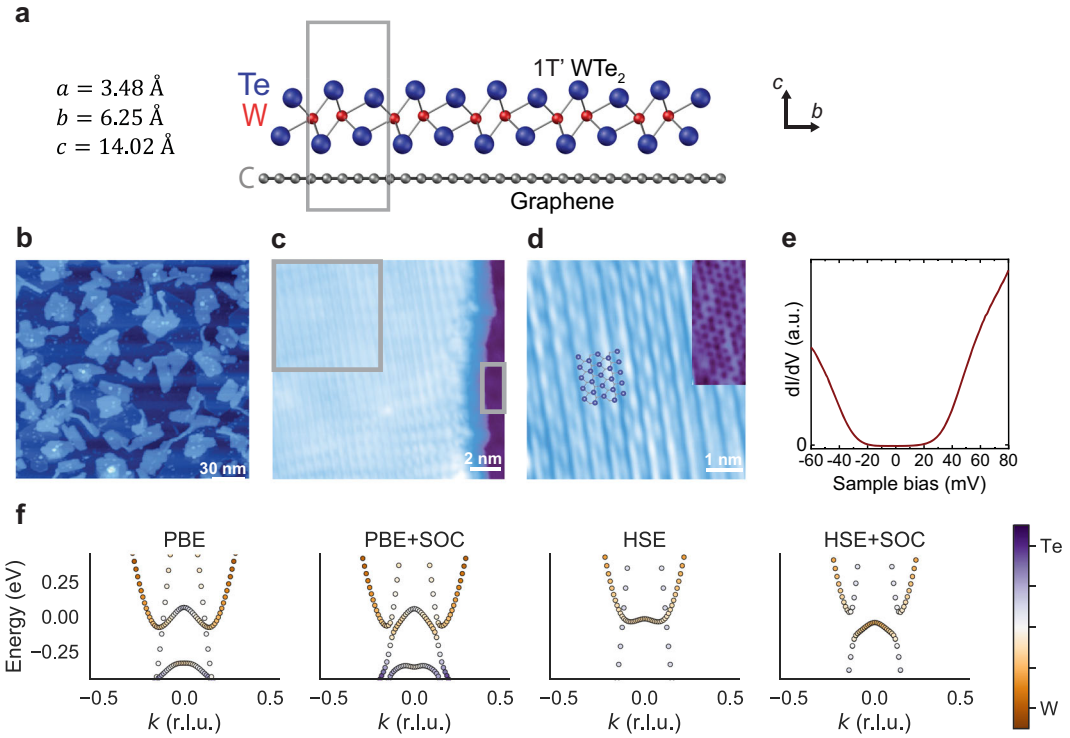

Fig. 1 Crystal structure and electronic structure of ML-WTe_2 films. a Crystal structure of monolayer 1 T′-WTe_2. **b** A typical large-scale topography of MBE-grown monolayer WTe_2 on graphene on SiC. **c**, **d** Zoomed-in topographies of monolayer islands showing characteristic Te stripes with atomic resolution. The graphene substrate can be identified to the right of the island in (**c**). **e** STS spectrum on the interior of one of the islands of the monolayer showing a gap of ~40 meV. **f** Calculated band structures of ML-WTe_2 (naive and DFT-calculated including spin-orbit coupling with PBE and HSE potentials respectively).

DFT calculations

To compare the experimentally measured gap to standard band theory calculations, we carry out DFT calculations using the Perdew–Burke–Ernzerhof (PBE)[15] and Heyd–Scuseria–Ernzerhof exchange-correlation functional (HSE06)[16] with and without spin-orbit interactions to compute the electronic structure of monolayer WTe_2. The results are summarized in Fig. 1f. As is common for small gap semiconductors such as Ge, PBE obtains a negative gap, while HSE06 obtains a gap of around 60 meV, within the range of the experimental observations. The bands are inverted due to SOC according to HSE06, and thus we expect the existence of topological helical edge states.

As a benchmark for the topological electronic structure, we identify the bulk and edge states of an island (shown in Fig. 2a) with no applied gate voltage. Upon tracking the spectra from the center of the island to the edge, we observe a bulk insulating gap and an emergence of a finite density of states in the nominal insulating gap as the tip approaches the edge. The in-gap density of states arises from the helical edge modes expected for a QSH insulator. The edge modes can be seen more clearly in d*I*/d*V* maps shown in Fig. 2d, thus confirming the existence of states which are highly localized to the edge near the Fermi energy, which we assign to be helical QSH edge states. We find that the spatial extent of the edge modes increases as the energy of the modes approaches the bulk band edges. This trend can be seen on both sides of the Fermi energy as plotted in Fig. 2c. This is an expected feature since topological edge modes must eventually merge into the bulk bands at a point beyond which their localization length diverges[17,18]. In our data, we find that the edge states are maximally localized at the Fermi level and merge into the bulk at the conduction band minima (CBM) and valence band maxima (VBM) values.

Further characterization of the ML-WTe_2 films shows that the bulk gap varies considerably from island to island (Fig. 3b–d). As measured by the difference between the CBM and VBM ($E_g = E_{cbm}$-E_{vbm}), the bulk gap can vary between 0 meV and 60 meV for different islands within the same film. The gap is however quite homogeneous within any given island as shown in Supplementary Fig. 3c. This large variation in gap sizes on different islands is not easy to explain, especially since the topographies of areas exhibiting different gaps show no differences in structure or defect concentration. A survey of the literature shows similarly large variations in gap magnitudes between different samples with no consensus on the low temperature gap. A recent study suggests that large strains can lead to gap variations in this system[19]. However, the samples in that study were deliberately grown to induce strain which is not the case for our samples or other reports. Another possible explanation is that the gap variations arise from trapped ions in the SiC substrate creating local electric fields. Such trapped ions have been previously observed in other films grown on SiC[20] and could result from the high energy RHEED electrons used to monitor film growth. So, while our measurements substantiate earlier conflicting experimental determinations of the band gap magnitude, the causes of the variations in gap magnitude remain unknown. Using the gated-STM capability we can systematically investigate the origin of these gap variations by measuring the response of ML-WTe_2 to electric fields.

Effect of gating on band structure

Our gating setup is shown in Fig. 4a where ML- WTe_2 was grown via MBE on chemical-vapor-deposited (CVD) graphene transferred onto 300 nm SiO_2/Si, with the Si substrate serving as the back gate electrode (see Methods and Supplementary Fig. 1 for details). Figure 4c, d shows a topographical STM image of a representative

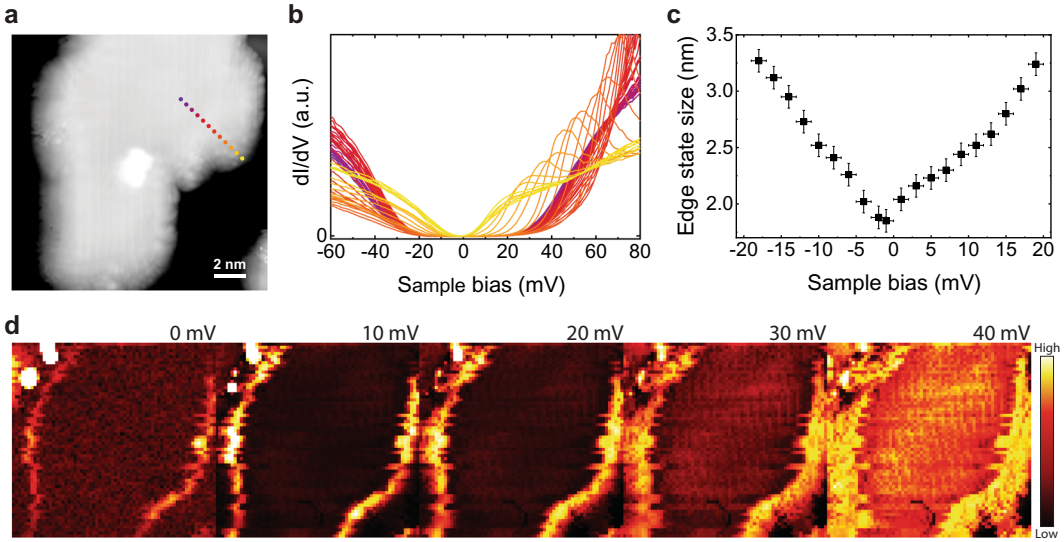

Fig. 2 Topological edge states in ML-WTe_2 and their spatial characteristics. a Topography of one of the monolayer islands. The colored dots are the spatial locations where the corresponding spectra shown in (**b**) were obtained. **b** d*I*/d*V* spectra corresponding to the dot positions in (**a**). **c** Spatial extent of the edge state (a few representative energies are shown in **d**) for different STM biases. The size is determined by choosing a d*I*/d*V* cut-off of 2% of the bulk spectrum value at 80 mV. The error bars were determined by the spatial resolution of the d*I*/d*V* map in (**d**), and bias modulation used to obtain the d*I*/d*V* spectra. **d** Spatially resolved local density of states (d*I*/d*V*) maps of the island shown in (**a**) at the indicated energies. The maps show continuous edge states along the edge, at all energies inside the gap, with a spatial extent that increases with energy.

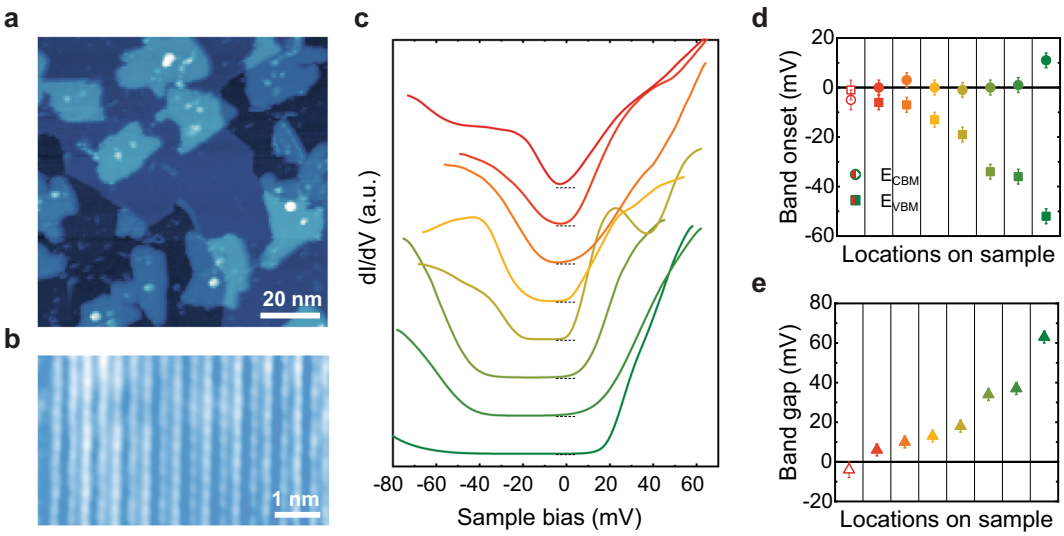

Fig. 3 Band gap variations in ML-WTe_2 film grown on graphene on SiC. a Typical large scale STM topography of ML-WTe_2 films. **b** Atomically resolved image of one of the monolayer islands. **c** d*I*/d*V* spectra taken on the same sample arranged in the order of decreasing band gap. The spectra shown were taken from monolayer islands without any visible defects from different, randomly chosen 1 μ-size locations on the 4 × 5 mm sample (see Supplementary Fig. 4). **d**, **e** Conduction band minimum (CBM), valence band maximum (VBM) (**d**), and band gap (**e**) plotted for the spectra shown in (**c**).

WTe_2 island on graphene on SiO_2. With this setup, we can apply positive and negative back gate voltages up to a maximum of 80 V. Naively, we expect that the applied electric field would simply modify the carrier concentration resulting in a rigid shift of the Fermi level relative to the bulk bands. The signature of this effect would be a rigid shift of the measured d*I*/d*V* spectrum relative to the Fermi energy. As shown in Fig. 4b, we find that gating does indeed move the Fermi energy toward the conduction/valence band consistent with electron/hole doping for positive/negative voltages respectively. However, gating has another, more dominant effect. As shown in Fig. 4b, e, f, with increasing positive gate voltage the band gap increases, while for negative gate voltages the band gap decreases. Hence, we find an inherent sensitivity of the WTe_2 insulating gap to (even modest) electric fields. At face value, it appears that positive and negative voltages have opposite effects on the gap. However, we will show below that this observed behavior is because the STM signal is dominated by the density of states from the top layer of the sample. In reality, both signs of the gate voltage decrease the net band gap.

Tight-binding model

To gain an understanding of these gating-induced band structure changes, (see methods section), we fit a tight-binding model to

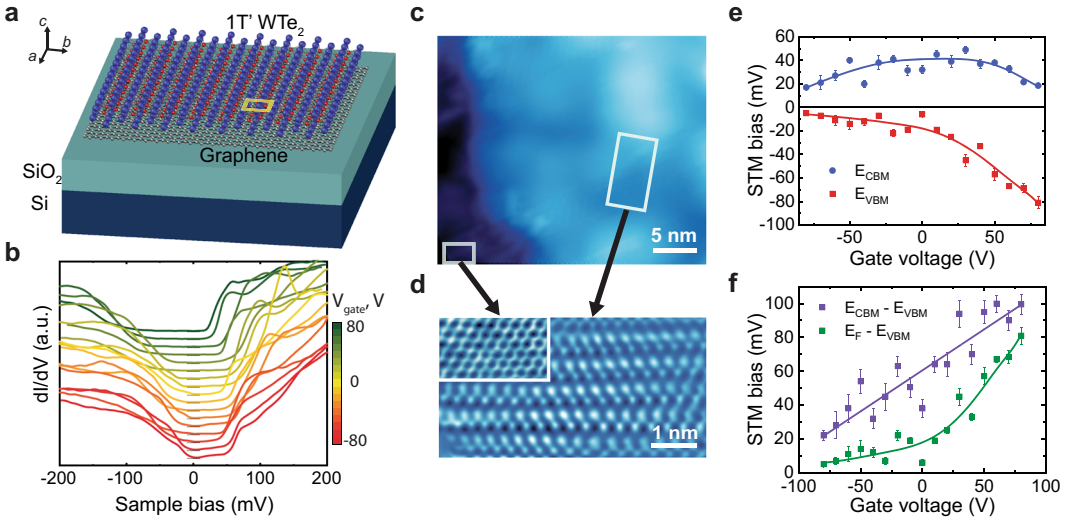

Fig. 4 Back-gated STM measurements of ML-WTe_2 on graphene on SiO_2. a Schematic of the back-gating setup. **b** Evolution of the bulk d*I*/d*V* spectrum of a monolayer island in response to the gate voltage. **c** STM image of monolayer WTe_2 island on graphene on SiO_2. **d** A zoom-in with atomic resolution showing Te atoms as well as the graphene lattice (inset). **e** Plots of the conduction band minimum and the valence band maximum for each spectrum at the given gate voltage (blue and red dots respectively) showing the non-trivial evolution of the bulk electronic structure with gate voltage. The blue and red lines are guides to the eye. The error bars are determined by the energy intervals at which data were obtained and the noise level of the d*I*/d*V* spectra. **f** Same as (**e**) but with energies relative to the VBM. Back-gating changes the band gap (violet dots) as well as the position of the VBM with respect to E_F (green dots). The violet and green lines are guides to the eye.

the DFT band structure using Wannier interpolation for our analysis. At zero gate electric field (see second panel of Fig. 5a), the CBM are doubly degenerate at $k_\pm \simeq \pm\left(0.15\frac{2\pi}{a}, 0\right)$. At k_+, the spin ↑ electron (i.e., the spin pointing in the z-direction) is localized on the top Te atom due to strong spin orbit coupling, while the spin ↓ electron is localized on the bottom Te atom. Consistent with time-reversal symmetry, this is reversed in the k_- direction, as noted on the diagram.

Next, we model the applied electric field by adding a term $(H\prime)$ to the tight-binding model, $H = H_0 + H' = H_0 + \sum_i eE \cdot z_i$, where z_i represents the *z*-coordinate of the *i*th Wannier center, computed as the expectation value of the position operator on the Wannier function. Figure 5a shows the 2D bulk band structures for different applied gate electric fields, and we see that the electric field breaks the spatial inversion symmetry and spin-splits the doubly degenerate CBM at $k_\pm \simeq \pm\left(0.15\frac{2\pi}{a}, 0\right)$. The spin-splitting is consistent with preserved time-reversal, but broken inversion symmetry. For negative gate voltages the conduction band minimum in the k_+ direction has spin ↓, while the minimum in the k_- direction has spin ↑. For the opposite electric field, this situation is reversed. From our model, an applied electric field always *reduces* the (indirect) band gap, irrespective of the sign of the gate voltage. To explain the STM gate dependence, we consider the density of states on the top layer. In Fig. 5a, the bands are colored according to the projection of the electronic states onto the top Te atoms, which we expect to be the most accessible to the STM probe. For a negative gate voltage, the states in the conduction band near $k_\pm$ that are pushed downward by the spin splitting are primarily located on the top Te atoms while the states pushed upward are primarily on the bottom Te atoms. For positive gate voltage, the situation is reversed. Since we expect the STM to have a preferential coupling to the top Te atoms this scenario predicts that the STM-observed gap should decrease for negative gate and increase for positive gate, in clear alignment with the experimental results.

In Fig. 5b, c we plot the gap and the calculated dI/dV spectra projected on the top Te atoms, as a function of electric field. The spectra are obtained by calculating the projected density of states (PDOS) of the Wannier functions of only the top Te atoms, i.e., $dI/dV|_\epsilon \propto \sum_i |\langle\phi_i|\psi\rangle|^2$, where *i* runs through all the Wannier orbitals of the top Te atoms. The results of the calculations shown in Fig. 5b, c agree well with the behavior of the experimentally measured gap with electric field as shown in Fig. 4f. For the 300 nm SiO_2 gate oxide, the 80 V gate voltage results in an electric field on the order of 100 mV Å^{-1}. A more accurate determination of the electric field strength is difficult because the thickness of the SiO_2 can show variations and graphene can induce some degree of screening. Nevertheless, using the value of 100 mV Å^{-1} as an estimate, we find that the change in the bulk gap with gate voltage (as measured from the top surface) to be 0.377(4) meV mV^{-1}, which is in excellent agreement with the experimental value of 0.39(2) meV mV^{-1}.

As an additional check, we confirm this mechanism for the decrease in gap magnitude with gate electric field by considering a minimal four-band tight-binding model constructed from a crystal symmetry analysis and fitted to first-principles calculations of the band structure[21]. Consistent with the DFT-derived tight-binding model, we find that the spin-splitting of the conduction band by the electric field is responsible for the observed behavior of the gap. We discuss this minimal model and present calculations of the surface gap electric field dependence in the Supplementary Information.

Our work highlights the sensitivity of the band structure of monolayer 1 T′-WTe_2 to electric fields, which cause large changes in the magnitude of the bulk band gap. Electronic structure calculations show that the effects due to electric fields can be primarily attributed to broken inversion symmetry and strong spin-orbit coupling akin to the Rashba effect, rather than electron-electron interaction effects. These systematic studies resolve the puzzlingly large variations in the gap magnitudes that have been previously observed in monolayer 1 T′-WTe_2 (see Supplementary Fig. 3). Indeed, we expect that the gap variations observed in the literature in the monolayer thin films may be attributed to electric fields arising from variations in the local potential induced by the substrate. This is consistent with our STM data on monolayer films grown without RHEED, which show far smaller variations in gap

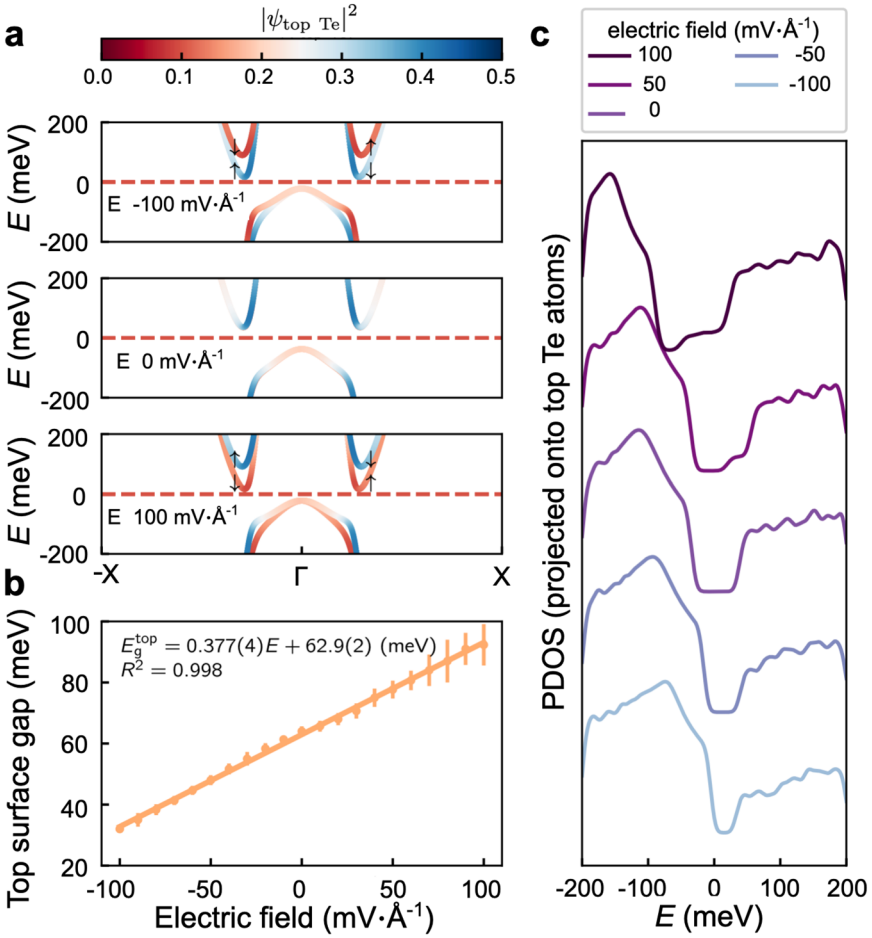

Fig. 5 Tight-binding calculations of the band structure and gating response of ML-WTe_2. a Band structure for −100, 0 and 100 mV Å^{-1} electric fields. We estimate that a gate voltage of 80 V corresponds to ~100 mV Å^{-1} The bands are colored with blue or red to represent electronic states that are more localized at the top Te atoms or the bottom Te atoms, respectively. The small black arrows indicate the spin polarization of the bands (near the band bottoms) due to the electric field from the applied gate voltage. **b** The computed gap at the top surface plotted versus the electric field. The slope and values are in close agreement with the STM data. **c** Projected density of states (PDOS) with different gate voltages. The PDOS represents the density of states projected onto the top Te atoms.

magnitude as shown in Supplementary Fig. 4c. Finally, it is worth highlighting our finding that the gate electric field can generate a spin-splitting of tens of meV in the 2D bulk bands. This substantial spin-splitting provides a new avenue to realizing proximity induced non-trivial superconductivity and Majorana bound states in a tunable system.

METHODS

Film growth

Graphene-on-SiC substrates were fabricated directly on crystalline SiC in vacuum, providing a high-quality graphene surface for subsequent epitaxial growth. WTe_2 films grown on graphene on SiC were transferred directly to the STM using a vacuum suitcase without exposure to air.

For gating studies, commercial graphene on SiO_2 substrates was used. These substrates were prepared by transferring monolayer CVD graphene onto a p-doped Si wafer coated with a 300 nm thermal SiO_2. Monolayer WTe_2 was grown using a custom MBE setup. Prior to growth, Gr/SiO_2/Si substrates were annealed in ultra-high vacuum (UHV) for 10 h at 450 °C. The film was grown by co-evaporation of elemental W (3 N purity) and Te (6 N purity) while the substrate was held at T = 280 °C. Te was evaporated from a Knudsen cell with a rate of 0.01 Å s^{-1}. W was evaporated using an electron beam evaporator at a rate of 0.18 Å h^{-1}. Monolayer film with 60% coverage was grown in 5 h, thus having the rate of approximately one monolayer per 8.5 h. Such slow growth and 200:1 Te to W flux ratio were necessary to grow high-quality monolayer films. After growth, the film was annealed in UHV at 300 °C for 1 h, cooled down to room temperature and capped with 15 nm of Te. The capped film was then transferred to the gating sample holder, which is a three-lead holder, one of which serves as the STM bias lead and the other two are connected to the heating W filament (see Supplementary Fig. 1). Once transferred to the STM system, the sample was ion-milled for 10 s using an Ar+ beam at 400 V voltage and 4 μA beam current and then annealed at 200 °C for 1 h to remove the Te cap. The samples were immediately transferred into the STM stage kept at 4 K.

DFT details

The DFT calculations are performed using Quantum ESPRESSO 6.5[22,23]. In order to compute the detailed band structure, we use Wannier interpolation. We derived a tight-binding model on a 56-spinor Wannier basis (W: *s* and *d*, Te: *s* and *p*) using Wannier90[24,25]. The tight-binding Hamiltonian is constructed and solved using the open-source code TBmodels[26].

DATA AVAILABILITY

All data presented in this work are available from the corresponding authors upon request.

Received: 1 June 2021; Accepted: 9 February 2022;
Published online: 18 March 2022

REFERENCES

1. Manzeli, S., Ovchinnikov, D., Pasquier, D., Yazyev, O. V. & Kis, A. 2D transition metal dichalcogenides. *Nat. Rev. Mat.* **2**, 17033 (2017).
2. Fei, Z. et al. Edge conduction in monolayer WTe_2. *Nat. Phys.* **13**, 677–682 (2017).
3. Tang, S. et al. Quantum spin Hall state in monolayer 1T′-WTe_2. *Nat. Phys.* **13**, 683–687 (2017).
4. Jia, Z.-Y. et al. Direct visualization of a two-dimensional topological insulator in the single-layer 1T′-WTe_2. *Phys. Rev. B* **96**, 041108 (2017).
5. Song, Y.-H. et al. Observation of Coulomb gap in the quantum spin Hall candidate single-layer 1T′-WTe_2. *Nat. Commun.* **9**, 4071 (2018).
6. Qian, X., Liu, J., Fu, L. & Li, J. Quantum spin Hall effect in two-dimensional transition metal dichalcogenides. *Science* **346**, 1344–1347 (2014).
7. Zheng, F. et al. On the quantum spin Hall gap of monolayer 1T′-WTe_2. *Adv. Mater.* **28**, 4845–4851 (2016).
8. Wu, S. et al. Observation of the quantum spin Hall effect up to 100 kelvin in a monolayer crystal. *Science* **359**, 76–79 (2018).
9. Shi, Y. et al. Imaging quantum spin Hall edges in monolayer WTe_2. *Sci. Adv.* **5**, eaat8799 (2019).
10. Novoselov, K. S. et al. Electric field effect in atomically thin carbon films. *Science* **306**, 666–669 (2004).
11. Xu, S.-Y. et al. Electrically switchable Berry curvature dipole in the monolayer topological insulator WTe_2. *Nat. Phys.* **14**, 900–906 (2018).
12. Sajadi, E. et al. Gate-induced superconductivity in a monolayer topological insulator. *Science* **362**, 922–925 (2018).
13. Fatemi, V. et al. Electrically tunable low-density superconductivity in a monolayer topological insulator. *Science* **362**, 926–929 (2018).
14. Lüpke, F. et al. Proximity-induced superconducting gap in the quantum spin Hall edge state of monolayer WTe_2. *Nat. Phys.* **16**, 526–530 (2020).
15. Perdew, J. P., Burke, K. & Ernzerhof, M. Generalized gradient approximation made simple. *Phys. Rev. Lett.* **77**, 3865–3868 (1996).
16. Heyd, J., Scuseria, G. E. & Ernzerhof, M. Hybrid functionals based on a screened Coulomb potential. *J. Chem. Phys.* **118**, 8207–8215 (2003).
17. Ok, S. et al. Custodial glide symmetry of quantum spin Hall edge modes in monolayer WTe_2. *Phys. Rev. B* **99**, 121105 (2019).
18. Lau, A., Ray, R., Varjas, D. & Akhmerov, A. R. Influence of lattice termination on the edge states of the quantum spin Hall insulator monolayer 1T′-WTe_2. *Phys. Rev. Mater.* **3**, 054206 (2019).
19. Zhao, C. et al. Strain tunable semimetal-topological-insulator transition in monolayer 1T′-WTe_2. *Phys. Rev. Lett.* **125**, 046801 (2020).
20. Krasheninnikov, A. V. & Nordlund, K. Ion and electron irradiation-induced effects in nanostructured materials. *J. Appl. Phys.* **107**, 071301 (2010).
21. Hu, M. et al. Realistic tight-binding model for monolayer transition metal dichalcogenides of 1T′ structure. *Phys. Rev. B* **104**, 035156 (2021).
22. Giannozzi, P. et al. QUANTUM ESPRESSO: a modular and open-source software project for quantum simulations of materials. *J. Phys. Condens. Matter* **21**, 395502 (2009).
23. Giannozzi, P. et al. Advanced capabilities for materials modelling with QUANTUM ESPRESSO. *J. Phys. Condens. Matter* **29**, 465901 (2017).
24. Pizzi, G. et al. Wannier90 as a community code: new features and applications. *J. Phys. Condens. Matter* **32**, 165902 (2020).
25. Mostofi, A. A. et al. An updated version of wannier90: a tool for obtaining maximally-localised Wannier functions. *Comput. Phys. Commun.* **185**, 2309–2310 (2014).
26. Gresch, D. TBmodels documentation. https://tbmodels.greschd.ch/en/latest/ (2020).

ACKNOWLEDGEMENTS

STM studies were supported by the U.S. Department of Energy (DOE), Office of Science, Office of Basic Energy Sciences (BES), Materials Sciences and Engineering Division under Award No. DE-SC0022101. Gating and MBE growth and characterization were supported by the Gordon and Betty Moore Foundation's EPiQS initiative through Grant No. GBMF9465. Y.C. and L. K. W. were supported by a grant from the Simons Foundation as part of the Simons Collaboration on the many-electron problem. The calculations made use of the computational resources provided by Illinois Campus Cluster and Blue Waters. M.R.H and T.H thank the US DOE for support under award DE-SC0020128. Y.C. thanks J. Zeng for discussions.

AUTHOR CONTRIBUTIONS

Y.M. and V.M. designed the experiments. Y.M., G.C., W.S. contributed to thin film growth. Y.M. carried out STM and gating studies and did the data analysis. Y.C., M.R.H., T.H., and L.W. did the theoretical modelling and calculations. All authors contributed to writing the paper.

COMPETING INTERESTS

The authors declare no competing interests.

ADDITIONAL INFORMATION

Supplementary information The online version contains supplementary material available at https://doi.org/10.1038/s41535-022-00433-x.

Correspondence and requests for materials should be addressed to Vidya Madhavan.

Reprints and permission information is available at http://www.nature.com/reprints

Publisher's note Springer Nature remains neutral with regard to jurisdictional claims in published maps and institutional affiliations.